Reducing Inter-Core Crosstalk Impact via Code-Interleaving and Bipolar 2-PPM for Core-Multiplexed SAC OCDMA PON

Ahmed E. A. Farghal and Hossam M. H. Shalaby

***Abstract*—Inter-core crosstalk (XT), caused by closely spaced cores, is the principal challenging issue of implementing multicore fiber (MCF)-based optical networks as it limits the network performance severely. In this paper, we propose and demonstrate using bipolar *M*-ary pulse position modulation (PPM) signaling in conjunction with the code-interleaving (CI) technique to address the inter-core XT problem in MCF-based optical code-division multiple-access (OCDMA) passive optical networks (PONs) with spectral-amplitude coding employed as the coding scheme. The bit error rate of the proposed network is derived based on an accurate analysis for the statistics of the decision random variables, i.e., mean and variance. The analysis accounts for inter-core XT, optical beat noise, and receiver noise. In addition, a comparison between the performance of core-multiplexed OCDMA PON adopting the newly proposed techniques, namely, unipolar on–off keying (OOK) with CI and bipolar 2-PPM with CI and that adopting unipolar OOK without CI, is presented under both data rate and average photons per bit constraints. The obtained results show that bipolar 2-PPM and CI are capable of reducing the inter-core XT impact on the performance of MCF-based OCDMA PONs. Furthermore, bipolar 2-PPM with CI outperforms other schemes in terms of the number of supportable users and energy efficiency.**

***Index Terms*—Inter-core crosstalk; Multicore fiber; OCDMA; Optical access; PPM.**

I. Introduction

In recent years, space-division multiplexing (SDM) techniques have attracted considerable attention for use in future passive optical networks (PONs) [1–6]. There exist multiple types of PON techniques, e.g., wavelength-division multiplexing PON [1,2], time-division multiple-access PON [3,4], orthogonal frequency-division multiplexing PON [5], and optical code-division multiple-access PON (OCDMA PON) [6]. These works show that combining SDM and PON techniques offers key benefits in terms of transmission capacity, optical network unit (ONU) scalability, split ratios, geographic coverage, and implementation cost.

OCDMA—with the advantages of asynchronous multiple accessibility with low-access delay, simple network control and management, all-optical processing, and enhanced confidentiality—is one promising candidate for future PONs [7]. Moreover, it provides symmetric downlink/uplink data rates [8] and quality-of-service differentiation at the physical layer level [9]. Using low-cost incoherent broadband light sources (BLSs) and complete cancellation of multiple-access interference (MAI) make spectral-amplitude coding (SAC) OCDMA of special interest [10]. Recently, a SDM/OCDMA hybrid PON based on uncoupled multicore fiber (MCF), called core-multiplexed OCDMA PON, which adopts SAC as a coding scheme with on–off keying (OOK) modulation, has been proposed [11]. Core-multiplexed OCDMA PON has been shown to be able to improve the capacity and scalability of OCDMA PONs. Nevertheless, core-multiplexed OCDMA PON has two major issues. First, at the required bit error rate (BER) level, there is always a subset of unused codes from the whole code family already generated when multiport encoders are employed, e.g., arrayed-waveguide-grating- (AWG) based encoders. Second, the inter-core crosstalk (XT), caused by the power coupling between signals during propagation in closely packed cores within a single fiber [12], contributes significantly to signal-dependent shot and beat noises and accordingly deteriorates the system performance [11].

In this paper, we propose and demonstrate using bipolar *M*-ary pulse position modulation (PPM) signaling in conjunction with the code-interleaving (CI) technique to address the inter-core XT and unused codewords problems in MCF-based OCDMA PONs with SAC employed as the coding scheme. In the CI technique, adjacent cores of MCF are assigned different unused code subsets in an interleaving manner with the desired core. On the other hand, employing PPM typically minimizes the interaction time between copropagating signals in neighboring cores since transmission takes place only in a fraction of the frame duration (i.e., slot time). However, a bandwidth penalty will be incurred to achieve the requirements on the data rate [13,14]. One approach to overcome this problem is to employ bipolar 2-PPM signaling for which the pulse position multiplicity *M* is set to 2, while each user is assigned two orthogonal codewords (i.e., bipolar complementary code

Manuscript received August 22, 2017; revised October 21, 2017; accepted October 30, 2017; published December 27, 2017 (Doc. ID 305377).

A. E. A. Farghal (e-mail: ahmed.farghal@el-eng.menofia.edu.eg) is with the Department of Electronics and Electrical Communications Engineering, Faculty of Electronic Engineering, Menoufia University, Menouf 32952, Egypt.

H. M. H. Shalaby is with the Electrical Engineering Department, Faculty of Engineering, Alexandria University, Alexandria 21544, Egypt.

https://doi.org/10.1364/JOCN.10.000035

keying) to encode the bipolar $\{-1, +1\}$ logic levels [14]. Our main contributions in this paper are as follows.

- We propose a novel optical line terminal (OLT) architecture that exploits through the CI technique the unused codewords by allowing the same compact encoder to be shared by two or more cores. The proposed architecture uses fewer light sources and encoders, thereby achieving a cost-effective and power-efficient network.
- We also introduce bipolar 2-PPM signaling as an effective solution to address the inter-core XT issue in core-multiplexed SAC OCDMA PON.
- Closed-form BER expressions for the proposed techniques, namely, unipolar OOK with CI and bipolar 2-PPM with CI, are obtained based on accurate analysis for the decision current mean and variance. The analysis considers the impact of inter-core XT, beat noise, and receiver noise.
- For validation purposes, the work in [15] is extended to the case of core-multiplexed PON and then compared with our model.

The paper is structured as follows. In Section II, we describe the proposed core-multiplexed SAC OCDMA PON architecture employing CI and bipolar 2-PPM. In Section III, we perform an analytical study for BER evaluation of the proposed network. Section IV presents the numerical results, while Section V concludes this work.

II. Proposed Architecture

A. Core-Multiplexed SAC OCDMA PON Adopting CI and OOK Architecture

A typical core-multiplexed OCDMA PON architecture employing 3-core MCF without CI is shown in Fig. 1(a) with the OLT, at the central office, consisting of three sub-OLTs [11]. Each sub-OLT is comprised of a BLS and an AWG router. Using an $N \times N$ AWG router in combination with codes having cyclic properties, e.g., balanced incomplete block design (BIBD) codes, N codewords can be generated simultaneously. Following OOK modulation with user data, the modulated encoded signals for all users belonging to a sub-OLT are combined using a power combiner. Next, the signals from all sub-OLTs are core-multiplexed via a fan-in device. The MCF is employed as a feeder fiber, where each core is used for serving a different sub-PON in a different geographic area. After being transmitted over L km MCF, the multiplexed signals are demultiplexed using a fan-out device. On each core at the required BER level, only $K_s (\ll N)$ ONUs can be simultaneously active, i.e., $N - K_s$ already generated codes at the output of the AWG encoder are unused. This is mainly because of the impact of noises and inter-core XT [11]. At each core output, a $1{:}K_s$ splitter [conventional optical distribution network (ODN)] is used to deliver the received signal to each ONU.

Figure 1(b) shows the proposed core-multiplexed OCDMA PON employing CI. To exploit the unused $N - K_s$ codes at a certain BER level, the compact encoder can be

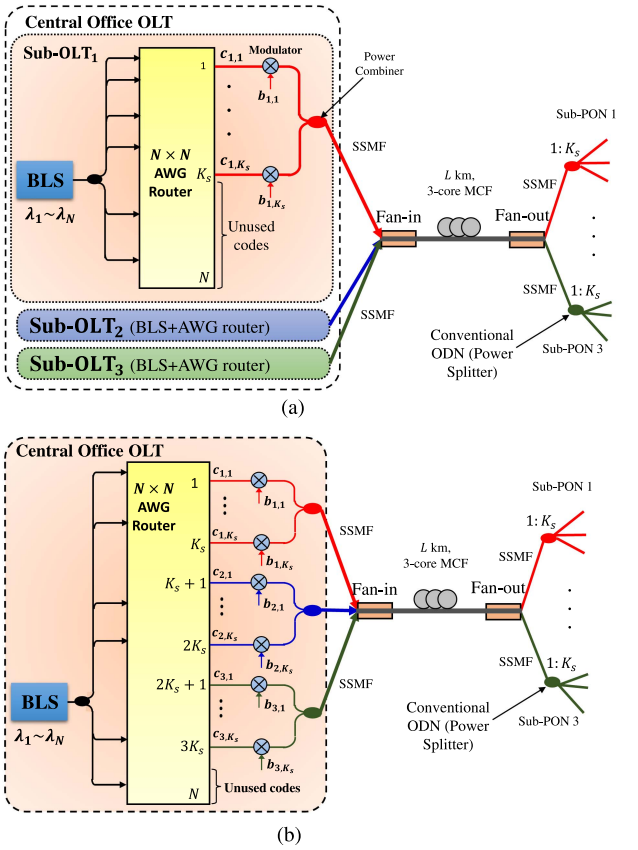

Fig. 1. OOK core-multiplexed SAC-OCDMA PON (a) without code-interleaving and (b) with code-interleaving.

shared by two or more cores by dividing the available N codes at the AWG output ports into two or more code subsets. The number of codewords in each code subset (i.e., code subset size K_s) depends on the required BER level. Each code subset is then designated to a specific sub-PON with the constraint that adjacent cores are assigned different code subsets. Assigning different code subsets to different cores in a manner that minimizes the number of compact encoders is equivalent to a graph coloring problem. Comparing Figs. 1(a) and 1(b), it is clear that introducing CI significantly reduces the OLT complexity since a lower number of light sources and encoders is needed, which substantially reduces the cost and power consumption. For the 3-core-based network example shown in Fig. 1(a), three BLSs and three $N \times N$ AWG encoders are needed, while by employing CI in Fig. 1(b), only one BLS and one $N \times N$ AWG encoder are needed.

B. Core-Multiplexed SAC OCDMA PON Adopting CI and Bipolar 2-PPM Architecture

Figure 2 shows the schematic of the proposed core-multiplexed SAC OCDMA PON adopting CI and bipolar 2-PPM. It is mainly composed of an OLT, a C-core MCF, an ODN, and a number of attached ONUs grouped in C sub-PONs.

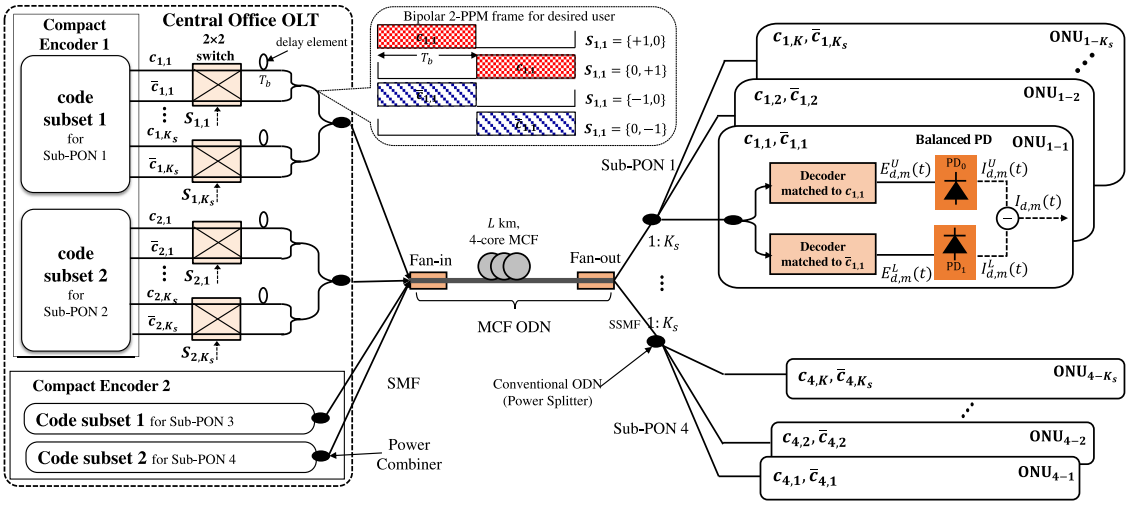

Fig. 2. Schematic architecture of core-multiplexed SAC OCDMA PON adopting CI and bipolar 2-PPM.

1) OLT Side: An OLT hosted in the central office comprises one or more compact OCDMA encoders based on AWG routers to provide the SAC codewords to the users (or ONUs) in different sub-PONs. In this paper, a modified prime sequence (MPS) code is employed as a signature sequence for bipolar 2-PPM [16]. The MPS code set has p code groups with p codewords in each group and is characterized by the tuple $(N = p^2, w = p, \lambda)$, with N, p, w, and λ representing the codeword length (also represents the code set size), prime number, codeword weight, and in-phase cross correlation, respectively. In fact, the choice of the MPS code set is because the sequences originating from different code groups have an ideal in-phase cross correlation, i.e., $\lambda = 1$, which implies lower beat noise impact. Moreover, the sequences sharing the same code group are orthogonal (i.e., $\lambda = 0$) and cyclic to each other. The orthogonal property makes MPS suitable for bipolar complementary code keying, while the cyclic property enables us to use cost-effective compact encoders based on AWG routers. A compact encoder architecture to generate the whole MPS code set can be realized via cascaded AWGs with low-port counts as in [17].

To implement the CI technique, the MPS code set of size $N(=p^2)$ is subdivided into N_s subsets of size $K_s = \lfloor \frac{p}{2N_s} \rfloor p$ orthogonal pairs each, dependent upon the required BER level, where $\lfloor \cdot \rfloor$ denotes the floor function. As shown in Fig. 2, each code subset is then dedicated to one of the sub-PONs connected to the OLT through one of the C cores of MCF so that no two adjacent cores have the same code subset. Table I shows an example of code assignment with CI for MPS with $p = 5$ and $N_s = 2$. If the number of code subsets is less than the number of MCF cores (i.e., $N_s < C$), the same code subsets (generated by another/other compact encoder/s) can be spatially reused in nonadjacent cores, e.g., compact encoder 2 in Fig. 2.

In the OLT, the transmitter of the k_ith ONU, $k_i \in \{1, 2, \ldots, K_s\}$, belonging to sub-PON $i \in \{1, 2, \ldots, C\}$, continuously generates statistically independent and identically distributed 2-ary binary data symbols $\boldsymbol{S}_{i,k_i}$s. The data symbol $\boldsymbol{S}_{i,k_i} = [s_{i,k_i,0} \quad s_{i,k_i,1}]$ takes values over the set $[\pm 1 \quad \pm 1]$. Each $\text{ONU}_{i-k_i}, i \in \{1, 2, \ldots, C\}, k_i \in \{1, 2, \ldots, K_s\}$ is assigned two orthogonal codewords from the same code group represented as $\boldsymbol{c}_{i,k_i} = [c_{i,k_i}^{(1)} \quad c_{i,k_i}^{(2)} \quad \cdots \quad c_{i,k_i}^{(N)}]$ and $\bar{\boldsymbol{c}}_{i,k_i} = [\bar{c}_{i,k}^{(1)} \quad \bar{c}_{i,k}^{(2)} \quad \cdots \quad \bar{c}_{i,k}^{(N)}]$. Here, $c_{i,k_i}^{(n)}, \bar{c}_{i,k_i}^{(n)} \in \{0, 1\}$ and the number of ns with $c_{i,k_i}^{(n)}$ (or $\bar{c}_{i,k_i}^{(n)}$) $= 1$ equals w. Moreover, for any $n \in \{1, 2, \ldots, N\}$, $c_{i,k_i}^{(n)} \bar{c}_{i,k_i}^{(n)} = 0$, i.e., $c_{i,k_i}^{(n)}$ and $\bar{c}_{i,k_i}^{(n)}$ are disjointed. If $+1$ is transmitted, $\boldsymbol{c}_{i,k_i}$ is used as the spreading sequence, and if -1 is transmitted, the complement code $\bar{\boldsymbol{c}}_{i,k_i}$ is used as the spreading sequence. Then, depending on the data symbol generated, the 2×2 optical switch will choose one of the

TABLE I
CI EXAMPLES FOR MPS WITH $p = 5$ AND $N_s = 2$

	Group	Code Sequences				
Core 1	0	$c_{1,1} = 10000$	10000	10000	10000	10000
	0	$\bar{c}_{1,1} = 00001$	00001	00001	00001	00001
	1	$c_{1,2} = 10000$	01000	00100	00010	00001
	1	$\bar{c}_{1,2} = 01000$	00100	00010	00001	10000
	2	$c_{1,3} = 10000$	00100	00001	01000	00010
	2	$\bar{c}_{1,3} = 00100$	00001	01000	00010	10000
	3	$c_{1,4} = 10000$	00010	01000	00001	00100
	3	$\bar{c}_{1,4} = 00010$	01000	00001	00100	10000
	4	$c_{1,5} = 10000$	00001	00010	00100	01000
	4	$\bar{c}_{1,5} = 00001$	00010	00100	01000	10000
Core 2	0	$c_{2,1} = 00010$	00010	00010	00010	00010
	0	$\bar{c}_{2,1} = 00100$	00100	00100	00100	00100
	1	$c_{2,2} = 00100$	00010	00001	10000	01000
	1	$\bar{c}_{2,2} = 00010$	00001	10000	01000	00100
	2	$c_{2,3} = 00001$	01000	00010	10000	00100
	2	$\bar{c}_{2,3} = 01000$	00010	10000	00100	00001
	3	$c_{2,4} = 01000$	00001	00100	10000	00010
	3	$\bar{c}_{2,4} = 00001$	00100	10000	00010	01000
	4	$c_{2,5} = 00010$	00100	01000	10000	00001
	4	$\bar{c}_{2,5} = 00100$	01000	10000	00001	00010

two incoherent coded (by the two orthogonal codes c_{i,k_i} and $\bar{c}_{i,k_i}$) light pulses to be further position modulated into one of the $M(=2)$ possible slots that constitute the bipolar 2-PPM frame (inset of Fig. 2). Hence, 2 data bits per symbol are encoded using $M_s = 2M$ symbols and accordingly incur no bandwidth penalty. Afterwards, it passively combined with the downlink modulated signals destined to other ONUs in sub-PON i and then coupled into core i using a fan-in device. This is repeated for the remaining $C-1$ sub-PONs.

2) ONU Side: After transmission through the L km C-core MCF link, the core-multiplexed combined signals are coupled out to C SMFs using a fan-out device. Each SMF $i \in \{1, 2, \ldots, C\}$ is equipped with a $1{:}K_s$ passive splitter for delivering the received signal to each ONU in the sub-PON i. The optical signal at the input of each ONU is optically split up into two parts. The upper arm signal is then decoded by a decoder matched to c_{i,k_i}, while the lower arm signal is decoded by a complement decoder, i.e., matched to $\bar{c}_{i,k_i}$. The two decoded signals are then photodetected using a pair of balanced photodetectors (PDs). Next, the balanced PD differentiated electrical output signal is integrated over slot duration T_b and sampled at time instants $t \in \{T_b, 2T_b\}$ where the decision variable set $[I_{i,0}, I_{i,1}]$ is produced for the target user in sub-PON i. Finally, these decision variables are compared to decide the transmitted data symbol $\tilde{S}$ with the decision rule [14]

$$\tilde{S} = \begin{cases} \boldsymbol{b}_i^{m,+}; & \text{if } I_{i,m} > |I_{i,\ell}|, \ell \neq m, \\ \boldsymbol{b}_i^{m,-}; & \text{if } I_{i,m} < -|I_{i,\ell}|, \ell \neq m, \end{cases} \tag{1}$$

where $\boldsymbol{b}_i^{m,\pm} = [\, b_{i,0}^m \quad b_{i,1}^m \,]$ with $b_{i,m}^m = \pm 1$ and $b_{i,l}^m = 0$ for $l \neq m$. Note that employing bipolar 2-PPM and CI adds no complexity in the ONUs, compared with using OOK SAC OCDMA [11].

C. Inter-Core XT

During propagation through the MCF link, the signals on each core are affected by inter-core XT from other cores, which may give rise to system performance deterioration [11]. SAC requires using BLSs with bandwidths so large that the inter-core interactions are approximately constant within the bandwidth of the light signal [18]. As a result, the inter-core XT impact is modeled as an additional noise component in the following analysis. In this paper, the inter-core XT from nonadjacent cores is ignored since the inter-core XT from adjacent cores dominates the total inter-core XT [19,20]. For the sake of convenience, we denote $\mathcal{G}$ as the set of core d and its adjacent cores and $\mathcal{H}$ as the set $\mathcal{G} - \{d\}$. Let $\Gamma_{ij}, i, j \in \mathcal{G}$ denote the fraction of power coupled into desired core i from undesired core j (note that $\Gamma_{ij} = 1$ for $j = i$). Using coupled-power theory and ignoring XT from nonadjacent cores, $\gamma_{ij}, j \neq i$, will be [11,12,19]

$$\Gamma_{ij}(L) = \frac{1 - e^{-(n_a+1)\mu_{\mathrm{XT}}}}{1 + n_a e^{-(N_a+1)\mu_{\mathrm{XT}}}}, \tag{2}$$

where n_a is the number of cores in $\mathcal{H}$ (i.e., the number of adjacent cores) and $\mu_{\mathrm{XT}} = 2\kappa^2 RL/\beta\Lambda$ is the mean of the XT [12]; κ, R, β, and Λ respectively represent the mode-coupling coefficient, the MCF bending radius, the propagation constant, and the core pitch. In the next section, we present the performance analysis of the proposed systems.

III. BER Performance Analysis

A. BER of Bipolar 2-PPM With a CI System

Without any loss of generality, we consider the first user in the desired sub-PON denoted as d as the intended user, which is assumed to be always active. Moreover, we assume that the symbol $s_{d,1} = \boldsymbol{b}_d^{0,+}$ is transmitted. For equiprobable data symbols, the bit-error probability BER_d for the bipolar 2-PPM system averaged over the desired core d and its adjacent cores, i.e., over set $\mathcal{G}$, is modified from [14], Eq. (24), as follows:

$$\mathrm{BER}_d = \frac{M_s}{2(M_s-1)} \times \sum_{g\in\mathcal{G}} \sum_{t_g \in t} \sum_{\ell_g \in \mathcal{L}} P_{\mathrm{e}|s_{d,1},\mathcal{K},T}(\boldsymbol{b}_d^{0,+}, \mathcal{L}, t) P_{\mathcal{K}}(\mathcal{L}), \tag{3}$$

where the interference matrix $\mathcal{L} \in \mathbb{N}^{(n_a+1)\times M}$ is defined as

$$\mathcal{L} \coloneqq \Bigg[\ell_g = (\ell_{g,0}, \ell_{g,1}, \ldots, \ell_{g,M-1}) \colon \quad \forall\, g \in \mathcal{G}, \ell_{g,m} \in \{0, 1, \ldots, K_g - t_g\}, \sum_{m=0}^{M-1} \ell_{g,m} = K_g - t_g \Bigg], \tag{4}$$

where $\mathbb{N}$ is the set of natural numbers and $\ell_{g,m}, g \in \mathcal{G}, m \in \{0, 1, \ldots, M-1\}$ represents the number of users belonging to sub-PON g that interfere with slot m of the desired user in sub-PON d and $t \coloneqq [t_g \colon \forall\, g \in \mathcal{G}]$, where t_g represents the realization of the number of active ONUs in the first code group in the code subset allocated to the gth sub-PON. At a time, only K_g ONUs in sub-PON g out of K_s are active and the other $K_s - K_g$ ONUs are idle. Since all the cores (sub-PONs) are independent, the probability distribution function (PDF) of t can be modified from [14], Eq. (4), to account for the core-multiplexed case as

$$P_T(t) = \frac{\binom{\lfloor \frac{p}{2} \rfloor - 1}{t_d - 1} \binom{K_s - \lfloor \frac{p}{2} \rfloor}{K_d - t_d}}{\binom{K_s - 1}{K_d - 1}} \prod_{h\in\mathcal{H}} \frac{\binom{\lfloor \frac{p}{2} \rfloor}{t_h} \binom{K_s - \lfloor \frac{p}{2} \rfloor}{K_h - t_h}}{\binom{K_s}{K_h}}, \tag{5}$$

where $\max\{1, \lfloor \frac{p}{2} \rfloor + K_d - K_s\} \leq t_d \leq \min\{\lfloor \frac{p}{2} \rfloor, K_d\}$ and $\max\{0, \lfloor \frac{p}{2} \rfloor + K_g - K_s\} \leq t_h \leq \min\{\lfloor \frac{p}{2} \rfloor, K_g\}$ for $h \in \mathcal{H}$.

Since $\ell_{g,m}, g \in \mathcal{G}, m \in \{0, 1, \ldots, M-1\}$ follows a binomial probability distribution characterized by $\ell_{g,m} \sim B(K_g - t_g, 1/M)$, where vector $\ell_g, g \in \mathcal{G}$ follows a multinomial probability distribution. In the proposed architecture, the users in different cores (sub-PONs) are statistically independent, so we have

$$P_{\mathcal{K}|\boldsymbol{T}}(\mathcal{L}|\boldsymbol{t}) = \prod_{g\in\mathcal{G}} \frac{(K_g - t_g)!}{\ell_{g,0}!\ell_{g,1}!\ldots\ell_{g,M-1}!}\left(\frac{1}{M}\right)^{K_g - t_g}. \tag{6}$$

Using the PDF of $\boldsymbol{t}$, we have

$$P_{\mathcal{K}}(\mathcal{L}) = P_{\mathcal{K}|\boldsymbol{T}}(\mathcal{L}|\boldsymbol{t})P_{\boldsymbol{T}}(\boldsymbol{t}). \tag{7}$$

Finally, assuming that noise is Gaussian-distributed,

$$P_{\mathrm{e}|S_{d,1},\mathcal{K},\boldsymbol{T}}(b_d^{0,+},\mathcal{L},\boldsymbol{t}) = Q\left[\frac{\mu_I(0,\boldsymbol{b}_d^{0,+}) - \mu_I(1,\boldsymbol{b}_d^{0,+})}{\sqrt{\sigma_I^2(0,\boldsymbol{b}_d^{0,+},\mathcal{L}) + \sigma_I^2(1,\boldsymbol{b}_d^{0,+},\mathcal{L})}}\right], \tag{8}$$

where $Q(x) = (1/2)\mathrm{erfc}(x/\sqrt{2})$, while $\mu_I(m,\boldsymbol{b}_d^{0,+})$ and $\sigma_I^2(m,\boldsymbol{b}_d^{0,+},\mathcal{L})$, $m = 0,1$, are the mean and variance of the random decision variable $I_{d,m}$ (see Fig. 2), respectively, which will be derived in the next subsubsections.

1) Upper-Arm Current Statistics: For convenience, all users are assumed to have the same peak received power of P_p. The received optical field of the mth slot, $m \in \{0,1\}$, at the upper PD (i.e., PD_0) of the desired user in core d is expressed as

$$E_{d,m}^U(t) = \sum_{g\in\mathcal{G}}\sum_{k_g=t_g}^{K_g} E_{g,k_g,m}^U(t),$$
$$E_{g,k_g,m}^U(t) = \sqrt{\Gamma_{dg}P_d}\sum_{n=1}^{N}\zeta_{g,k_g,m}^{(n)}(t)c_{d,1}^{(n)}e^{j\varphi_{g,k_g}^{(n)}(t)}, \tag{9}$$

where from [14]

$$\zeta_{g,k_g,m}^{(n)}(t) = [\alpha_{g,k_g,m}c_{g,k_g}^{(n)} + \beta_{g,k_g,m}\bar{c}_{g,k_g}^{(n)}]\Pi\left[\frac{t - m\tau}{\tau}\right],$$
$$\alpha_{g,k_g,m} \coloneqq \frac{|s_{g,k_g,m}| + s_{g,k_g,m}}{2}, \quad \text{and}$$
$$\beta_{g,k_g,m} \coloneqq \frac{|s_{g,k_g,m}| - s_{g,k_g,m}}{2}. \tag{10}$$

Here, $\Pi[\cdot]$ is the signaling waveform, assumed to be of rectangular shape. $P_d = P_p/N$ is the optical power per spectral bin, $j = \sqrt{-1}$ is the imaginary operator, and $\varphi_{g,k_g}^{(n)}(t)$ is the random phase of the optical field of spectral bin $n \in \{1,2,\ldots,N\}$ of user $k_g \in \{1,2,\ldots,K_g\}$ in sub-PON $g \in \mathcal{G}$.

The decision variable at the output of the upper square-law PD (i.e., PD_0) of the target user in sub-PON d, on the mth slot, is adapted from [11] to account for both the CI scheme and PPM modulation as follows:

$$I_{d,m}^U = \frac{\Re}{T_b}\int_{mT_b}^{(m+1)T_b}\Bigg[|E_{d,1,m}^U(t)|^2 + \sum_{k_d=t_d+1}^{K_d}|E_{d,k_d,m}^U(t)|^2$$
$$+2\sum_{k_d=t_d+1}^{K_d}|E_{d,1,m}^U(t)||E_{d,k_d,m}^U(t)|\cos[\Delta\varphi_{d,1,d,k_d}^{(n)}(t)]$$
$$+2\sum_{\substack{k_d\,l_d=t_d+1\\ k_d>l_d}}^{K_d}|E_{d,k_d,m}^U(t)||E_{d,l_d,m}^U(t)|\cos[\Delta\varphi_{d,k_d,d,l_d}^{(n)}(t)]$$
$$+\sum_{h\in\mathcal{H}}\Bigg\{2\sum_{k_h=t_h}^{K_h}|E_{d,1,m}^U(t)||E_{h,k_h,m}^U(t)|\cos[\Delta\varphi_{d,1,h,k_h}^{(n)}(t)]$$
$$+\sum_{k_d=t_d+1}^{K_d}\sum_{l_h=t_h}^{K_h}|E_{d,k_d,m}^U(t)||E_{h,l_h,m}^U(t)|\cos[\Delta\varphi_{d,k_d,h,l_h}^{(n)}(t)]$$
$$+2\sum_{\substack{k_h\,l_h=t_h\\ k_h>l_h}}^{K_h}|E_{h,k_h,m}^U(t)||E_{h,l_h,m}^U(t)|\cos[\Delta\varphi_{h,k_h,h,l_h}^{(n)}(t)]$$
$$+\sum_{k_h=t_h}^{K_h}|E_{h,k_h,m}^U(t)|^2\Bigg\}\Bigg]\mathrm{d}t, \tag{11}$$

where $\Re$ is the PD responsivity and $\Delta\varphi_{i,k_i,j,l_j}^{(n)}(t) = \varphi_{i,k_i}^{(n)}(t) - \varphi_{j,l_j}^{(n)}(t)$, $i,j \in \mathcal{G}$. The first, second, and last terms on the right-hand side of Eq. (11) are, respectively, the desired signal, the intra-core MAI signal, and the inter-core MAI signal resulted from cores belonging to the set $\mathcal{H}$. The third and fifth terms are the first-order beat noise terms between the signal and intra-interferers in core d and between the signal and inter-interferers (due to XT). The fourth, sixth, and seventh terms are the second-order beat noise terms between interferer–interferer, interferer–XT, and XT–XT, respectively. It is noteworthy that by employing CI, the inter-core XT MAI and the first-order beat noise terms due to using the same codes on adjacent cores are eliminated compared to the scheme in [11], Eq. (9).

In Eq. (11), for $i \in \mathcal{G}$,

$$\frac{1}{T_b}\int_{mT_b}^{(m+1)T_b}|E_{i,k_i,m}^U(t)|^2\mathrm{d}t$$
$$= \Gamma_{di}P_d\sum_{n=1}^{N}c_{d,1}^{(n)}[\alpha_{g,k_g,m}c_{g,k_g}^{(n)} + \beta_{g,k_g,m}\bar{c}_{g,k_g}^{(n)}], \tag{12}$$

where $\Gamma_{di} = 1$ for $i = d$. Moreover, for $i,j \in \mathcal{G}$,

$$\frac{1}{T_b}\int_{mT_b}^{(m+1)T_b}|E_{i,k_i,m}^U(t)||E_{j,l_j,m}^U(t)|\cos[\Delta\varphi_{i,k_i,j,l_j}^{(n)}(t)]\mathrm{d}t$$
$$= \sqrt{\Gamma_{di}\Gamma_{dj}}P_d\sum_{n=1}^{N}c_{d,1}^{(n)}[\alpha_{i,k_i,m}c_{i,k_i}^{(n)} + \beta_{i,k_i,m}\bar{c}_{i,k_i}^{(n)}]$$
$$\times[\alpha_{j,k_j,m}c_{j,k_j}^{(n)} + \beta_{j,k_j,m}\bar{c}_{j,k_j}^{(n)}]X_{i,k_i,j,l_j}^{(n)}(m), \tag{13}$$

where the random variable $X_{i,k_i,j,l_j}^{(n)}(m)$ for any $i,j \in \mathcal{G}$, any $k_i \in \{1,2,\ldots,K_i\}$, any $l_j \in \{1,2,\ldots,K_j\}$, and any $n \in \{1,2,\ldots,N\}$, with $l_j \neq k_i$ if $i = j$ and *vice versa* (i.e., $i \neq j$ if $l_j = k_i$) is defined as

$$X^{(n)}_{i,k_i,j,l_j}(m) \coloneqq \frac{1}{T_b}\int_{mT_b}^{(m+1)T_b} \Pi^2\left[\frac{t-m\tau}{\tau}\right]\cos[\Delta\varphi^{(n)}_{i,k_i,j,l_j}(t)]\mathrm{d}t. \tag{14}$$

The phase noises are zero-mean mutually independent Gaussian-distributed of Wiener–Lévy form [14,21], with variance $\sigma^2_{X^{(n)}_{i,k_i,j,l_j}(m)} \approx \tau_c B_e$, where $\tau_c = N/\Delta\nu$ is the BLS coherence time, $\Delta\nu$ is the light source linewidth, and $B_e = 1/(2T_b)$ is the electrical bandwidth of the receiver.

The cross correlation between two MPS sequences $\boldsymbol{c}_{i,k_i}$ and $\boldsymbol{c}_{j,l_j}$ for $i,j \in \mathcal{G}$, $k_i, l_j \in \{1,2,\ldots,K_s\}$ is given by

$$\sum_{n=1}^{N} c^{(n)}_{j,l_j} c^{(n)}_{i,k_i} = \begin{cases} w; & \text{for } i=j, k_i = l_j, \\ 0; & \text{for } i=j, k_i \neq l_j, \text{and codes} \\ & k_i \text{ and } l_j \text{ in the same group}, \\ \lambda; & \text{else.} \end{cases} \tag{15}$$

We define the interfering random variable as $\kappa_{d,m} \coloneqq \sum_{k_d=t_d+1}^{K_d} |s_{d,k_d,m}|, m \in \{0,1\}$, and the XT interfering random variable as $\kappa_{h,m} \coloneqq \sum_{k_h=t_h}^{K_h} |s_{h,k_h,m}|, h \in \mathcal{H}, m \in \{0,1\}$. Then, by exploiting Eq. (15), the statistics of $I^U_{d,m}$ are given by

$$\begin{aligned} \mu_{I^U_{d,m}} &\coloneqq \mathbb{E}[I^U_{d,m}] = \Re P_d\left[w\alpha_{d,1,m} + \lambda\kappa_{d,m} + \lambda\sum_{h\in\mathcal{H}}\Gamma_{dh}\kappa_{h,m}\right], \\ \sigma^2_{I^U_{d,m}} &\coloneqq \mathrm{Var}\{I^U_{d,m}\} = \mathbb{E}[|I^U_{d,m}|^2] - |\mathbb{E}[I^U_{d,m}]|^2 \\ &= 4B_e\tau_c(\Re P_d)^2\left[\lambda\alpha_{d,1,m}\sum_{g\in\mathcal{G}}\Gamma_{dg}\kappa_{g,m}\right. \\ &\quad + \frac{\lambda w}{N}\sum_{h\in\mathcal{H}}\Gamma_{dh}(\kappa_{d,m}\wedge\kappa_{h,m})(\kappa_{d,m}\vee\kappa_{h,m}-1) \\ &\quad \left. + \frac{\lambda w}{N}\sum_{g\in\mathcal{G}}\Gamma^2_{dg}\frac{\kappa_{g,m}(\kappa_{g,m}-1)}{2}\right], \end{aligned} \tag{16}$$

where $\mathbb{E}[\cdot]$ is the expectation operator, $x\wedge y \coloneqq \min\{x,y\}$, and $x\vee y \coloneqq \max\{x,y\}$.

2) Lower-Arm Current Statistics: The statistics of the random variable $I^L_{d,m}$ are derived following an analysis similar to that carried out for $I^U_{d,m}$ with $c^{(n)}_{d,1}$ in Eq. (9) replaced with $\bar{c}^{(n)}_{d,1}$. We have

$$\begin{aligned} \mu_{I^L_{d,m}} &= \Re P_d\left[w\beta_{d,1,m} + \lambda\kappa_{d,m} + \lambda\sum_{h\in\mathcal{H}}\Gamma_{dh}\kappa_{h,m}\right], \\ \sigma^2_{I^L_{d,m}} &= 4B_e\tau_c(\Re P_d)^2\left[\lambda\beta_{d,1,m}\sum_{g\in\mathcal{G}}\Gamma_{dg}\kappa_{g,m}\right. \\ &\quad + \frac{\lambda w}{N}\sum_{h\in\mathcal{H}}\Gamma_{dh}(\kappa_{d,m}\wedge\kappa_{h,m})(\kappa_{d,m}\vee\kappa_{h,m}-1) \\ &\quad \left. + \frac{\lambda w}{N}\sum_{g\in\mathcal{G}}\Gamma^2_{dg}\frac{\kappa_{g,m}(\kappa_{g,m}-1)}{2}\right]. \end{aligned} \tag{17}$$

3) Decision Current Statistics: The mean of the random decision variable $I_{d,m} = I^U_{d,m} - I^L_{d,m}$ over slot $m \in \{0,1\}$ given transmitted data symbol $\boldsymbol{s}_{d,1} = \boldsymbol{b}^{0,+}_d = [\,b^0_{d,0} \quad b^0_{d,1}\,] = [\,+1 \quad 0\,]$ is calculated as

$$\mu_I(m, \boldsymbol{b}^{0,+}_d) = \mu_{I^U_{d,m}} - \mu_{I^L_{d,m}} = \Re P_d w b^0_{d,m}. \tag{18}$$

It should be noted that the proposed architecture preserves the MAI cancellation capability of SAC OCDMA. The variance of the total noise is given as

$$\sigma^2_I(m, \boldsymbol{b}^{0,+}_d, \mathcal{L}) = \sigma^2_{\mathrm{beat}|m,\boldsymbol{b}^{0,+}_d,\mathcal{L}} + \sigma^2_{\mathrm{sh}|m,\boldsymbol{b}^{0,+}_d,\mathcal{L}} + \sigma^2_T, \tag{19}$$

with the beat noise component

$$\sigma^2_{\mathrm{beat}|m,\boldsymbol{b}^{0,+}_d,\mathcal{L}} = \sigma^2_{I^U_{d,m}} + \sigma^2_{I^L_{d,m}}, \tag{20}$$

and the shot noise component

$$\sigma^2_{\mathrm{sh}|m,\boldsymbol{b}^{0,+}_d,\mathcal{L}} = 2eB_e[\mu_{I^U_{d,m}} + \mu_{I^L_{d,m}}], \tag{21}$$

where $e = 1.6\times10^{-19}$ C is the elementary charge. The additivity of noise variance contributions from detectors PD_0 and PD_1 in Eqs. (20) and (21) follows because the noises induced at the two photodetectors are statistically independent [22]. Finally, the thermal noise variance $\sigma^2_T = 4k_BT_nB/R_L$, with $k_B = 1.38\times10^{-23}$ J/°K being the Boltzmann's constant, T_n the receiver noise temperature, and R_L the receiver load resistance. In the case of no inter-core XT, i.e., $\Gamma_{dh} = 0$, $\forall\, h \in \mathcal{H}$, Eqs. (20) and (21) reduce to the single-core case expressions given in [14].

B. BER of Unipolar OOK With CI System

Employing a similar technique to that used in [11] and using Eq. (11) with $m = 0$ and $t_d = 1$, the average BER of core d ONUs for OOK with a CI-based network will be

$$\begin{aligned} \mathrm{BER}_d = \sum_{\ell_d=0}^{K_d-1}\sum_{\ell_h=0:h\in\mathcal{H}}^{K_h} &\frac{\binom{K_d-1}{\ell_d}}{2^{K_d-1}}\prod_{h\in\mathcal{H}}\frac{\binom{K_h}{\ell_h}}{2^{K_h}} \\ &\times Q\left(\frac{\mu_1-\mu_0}{\sigma_{\mathrm{tot}|1,\ell_d,\ell} + \sigma_{\mathrm{tot}|0,\ell_d,\ell}}\right), \end{aligned} \tag{22}$$

where $\mu_{b_d} = \Re P_d w b_d$, $b_d \in \{0,1\}$ is the binary data of the desired user in core d, and $\ell \overset{\mathrm{def}}{=} [\ell_h{:}\forall\, h \in \mathcal{H}, \ell_h \in \{0,1,\ldots,K_h\}]$ is the XT interfering random vector.

The total noise variance, $\sigma^2_{\mathrm{tot}|b_d,\ell_d,\ell}$, is given by

$$\sigma^2_{\mathrm{tot}|b_d,\ell_d,\ell} = \sigma^2_{\mathrm{sh}|b_d,\ell_d,\ell} + \sigma^2_{\mathrm{beat}|b_d,\ell_d,\ell} + \sigma^2_T, \tag{23}$$

where

$$\sigma^2_{\mathrm{sh}|b_d,\ell_d,\ell} = 2eB_e\Re P_d\left[wb_d + 2\sum_{g\in\mathcal{G}}\Gamma_{dg}\ell_g\lambda\right], \tag{24}$$

$$\sigma^2_{\text{beat}|b_d,\ell_d,\ell} = 4B_e\tau_c(\Re P_d)^2 \times \left[\lambda b_d \sum_{g\in\mathcal{G}}\Gamma_{dg}\ell_g + \frac{\lambda w}{N}\left\{\sum_{g\in\mathcal{G}}\Gamma^2_{dg}\frac{\ell_g(\ell_g-1)}{2} + \sum_{h\in\mathcal{H}}\Gamma_{dh}(\ell_d\wedge\ell_h)(\ell_d\vee\ell_h-1)\right\}\right] + 4B_e\tau_c(\zeta\Re P_d)^2\left(\lambda-\frac{\lambda w}{N}\right)\left[\sum_{g\in\mathcal{G}}\Gamma^2_{dg}\frac{\ell_g(\ell_g-1)}{2} + \sum_{h\in\mathcal{H}}\Gamma_{dh}(\ell_d\wedge\ell_h)(\ell_d\vee\ell_h-1)\right], \quad (25)$$

where $\zeta = \lambda/(w-\lambda)$ is the attenuation parameter required for MAI cancellation in the case of unipolar OOK.

For validation purposes, we extend the analysis presented in [15] to drive the BER for an OOK core-multiplexed SAC-OCDMA system with CI. As a benchmark, Hadamard codes $(N, w = N/2, \lambda = N/4)$ are used as signature sequences in this analysis because for this family of codes, the upper and lower bounds as well as the simulation results coincide with each other. Following [15], we have

$$\text{BER}_d = \sum_{\ell_d=0}^{K_d-1}\sum_{\ell_h=0:h\in\mathcal{H}}^{K_h}\frac{\binom{K_d-1}{\ell_d}}{2^{K_d-1}}\prod_{h\in\mathcal{H}}\frac{\binom{K_h}{\ell_h}}{2^{K_h}} \times\left[Q\left(\frac{wT_b\Re P_d-\theta}{\sigma_{b_d=1}(\ell_d,\ell)}\right)+Q\left(\frac{\theta}{\sigma_{b_d=0}(\ell_d,\ell)}\right)\right], \quad (26)$$

where θ is the threshold for the decision variable and

$$\sigma^2_{b_d=1}(\ell_d,\ell) = \lambda\frac{\ell_d(\ell_d+1)}{2}\sigma^2_{d,2} + \sum_{h\in\mathcal{H}}\lambda\frac{\ell_h(\ell_h-1)}{2}\sigma^2_{h,2} + \sum_{h\in\mathcal{H}}\lambda\ell_h(\ell_d+1)\sigma^2_{dh,2}, \quad (27)$$

$$\sigma^2_{b_d=0}(\ell_d,\ell) = \lambda\frac{\ell_d(\ell_d-1)}{2}\sigma^2_{d,2} + \sum_{h\in\mathcal{H}}\lambda\frac{\ell_h(\ell_h-1)}{2}\sigma^2_{h,2} + \sum_{h\in\mathcal{H}}\lambda\ell_h\ell_d\sigma^2_{dh,2} \quad (28)$$

with

$$\sigma^2_{g,2} \coloneqq \Re^2\Gamma^2_{dg}\int_0^T\int_0^T A^2(t_1)A^2(t_2)e^{-2\frac{|t_1-t_2|}{\tau_c}}\mathrm{d}t_1\mathrm{d}t_2 = 2\Re^2\Gamma^2_{dg}P_d^2T_b\tau_c\left(1-\frac{\tau_c}{2T_b}(1-e^{-2\frac{T_b}{\tau_c}})\right), \quad (29)$$

$$\sigma^2_{dh,2} \coloneqq \Re^2\Gamma_{dh}\int_0^T\int_0^T A^2(t_1)A^2(t_2)e^{-2\frac{|t_1-t_2|}{\tau_c}}\mathrm{d}t_1\mathrm{d}t_2 = 2\Re^2\Gamma_{dg}P_d^2T_b\tau_c\left(1-\frac{\tau_c}{2T_b}\left(1-e^{-2\frac{T_b}{\tau_c}}\right)\right), \quad (30)$$

where $A(t)$ is the envelope of the optical field, assumed to have rectangular shape.

IV. Results and Discussion

In order to maintain the same average photons per information bit μ_{ph} for all employed systems, the peak single-user received power will be given by

$$P_p = \begin{cases} 2\log_2(2)\eta\mu_{\text{ph}}R_b/\Re, & \text{for unipolar OOK,} \\ \log_2(2)\eta\mu_{\text{ph}}R_b/\Re, & \text{for bipolar OOK,} \\ \log_2(4)\eta\mu_{\text{ph}}R_b/\Re, & \text{for bipolar 2-PPM,} \end{cases} \quad (31)$$

where η is the PD efficiency, assumed to be unity. Moreover, the numerical results presented in this section are considered under a constraint on data rate per user R_b. The system parameters are $T_n = 300°\text{K}$, $R_L = 1\ \text{k}\Omega$, $\Delta\nu = 3.5$ THz, $\beta = 6$ rad/μm, and $R_b = R_b^{\text{OOK}} = R_b^{\text{PPM}} = 1$ Gbit/s.

We first consider the case of core-multiplexed SAC OCDMA PON adopting unipolar OOK signaling with and without CI. Figure 3 shows the average BER for BIBD $(N = 57, w = 8, \lambda = 1)$ codes as a function of the number of active ONUs per core for $\mu_{\text{ph}} = 2.2\times10^5$, $R = 0.4$ m, $\Lambda = 40$ μm, $\kappa = 0.04\ \text{m}^{-1}$, and $L = 50$ km. The results are shown for a desired core with two (e.g., 12-core with one-ring structure MCF [23]), three (e.g., outer core of 7-core with hexagonal structure MCF [24]), and six (e.g., outer core of 7-core with hexagonal structure MCF [24]) neighbors. From Fig. 3, a unipolar OOK-based network without XT (single-core case) can accommodate up to 16 active ONUs (≈28% of $N = 57$ available codes) at a reference BER of 10^{-9}. For the core-multiplexed OCDMA PON without CI [11], inter-core XT causes the BER to increase and the number of supportable ONUs to decrease. This degradation can be attributed to the inter-core XT contribution to both signal-dependent shot and beat noise variances (according to [11], Eqs. (22) and (24)). The center core of the 7-core MCF has the worst BER performance since it undergoes XT from

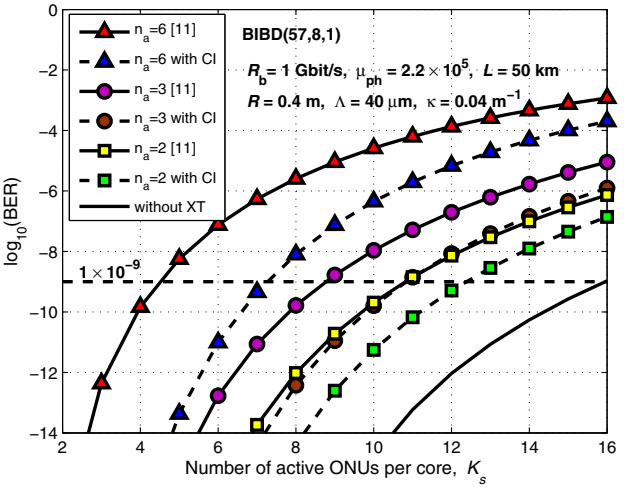

Fig. 3. Average BER of core-multiplexed SAC OCDMA PON adopting unipolar OOK versus the number of active ONUs.

six adjacent cores. On the other hand, the adaption of CI results in XT reduction and hence increases the number of supportable ONUs at the required BER level. For instance, the number of supported ONUs increases from 9 to 11 at BER $= 10^{-9}$ for a desired core with $n_a = 3$ when the CI technique is employed. This improvement can be attributed to the fact that as different codes are used on adjacent cores, the XT MAI and first-order beat noise due to using the same codes on adjacent cores are eliminated [see Eq. (11)].

Figure 4 plots the BER of OOK core-multiplexed SAC OCDMA PON with CI given in Eq. (22) for Hadamard ($N = 128, w = 64, \lambda = 32$) codes as a function of number of active ONUs per core. To validate the accuracy of our derived model, Fig. 4 also shows the BER given by the expression in Eq. (26) extended from [15]. It is clear that the analytical results obtained using Eq. (22) agree well with the results obtained using the extended expression, which justifies the correctness of the proposed model.

Figure 5 shows a comparison between the BER of unipolar OOK employing BIBD (183,14,1) codes and bipolar 2-PPM employing MPS (169,13,1) codes for the single-core case, i.e., without inter-core XT. It is obvious from the figure that at a reference BER of 10^{-9}, the unipolar OOK-based network can accommodate up to 20 active ONUs, whereas about 31 ONUs (representing about 39.7% of 78 orthogonal pairs available in the used MPS code set) can be accommodated in the case of the bipolar 2-PPM-based network. This performance gain will be employed to mitigate the impact of inter-core XT on the performance of core-multiplexed SAC OCDMA PON. Moreover, the unused codewords in the MPS code set at the required BER will be exploited through the CI technique. In addition, the BER of bipolar OOK adopting MPS (169,13,1) code is also included in Fig. 5. It is clear from the figure that using bipolar OOK gave no advantage compared to unipolar OOK but increased the OLT complexity as 2×2 switches are needed. Hereafter, we only consider the core-multiplexed network

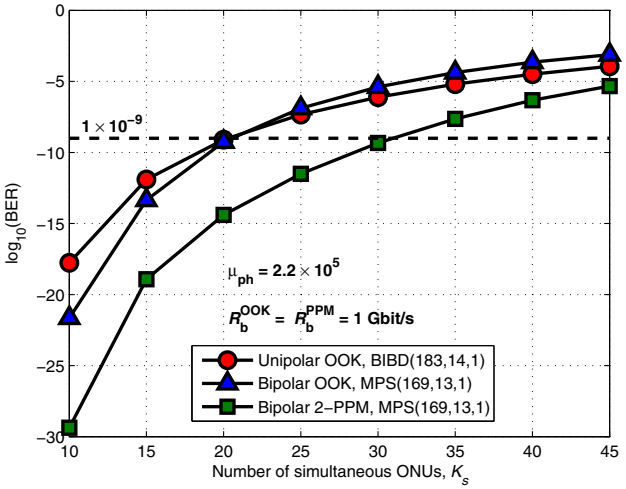

Fig. 5. Average BER of single-core SAC OCDMA PON versus the number of simultaneous ONUs.

for the cases of unipolar OOK with CI and bipolar 2-PPM with CI.

The average BER as a function of the number of active ONUs per core is shown in Fig. 6 for a desired core with $n_a = 3$ when $\mu_{\rm ph} = 2.2 \times 10^5$, $R = 0.4$ m, $L = 50$ km, and $R_b = 1$ Gbit/s. In the figure, the numbers in the parentheses represent mode-coupling coefficient κ in m^{-1} and core pitch Λ in μm, respectively. Three values of (κ, Λ) are considered: (0.002, 45), (0.04, 40), and (0.1, 35), corresponding to weak, moderate, and strong inter-core XT, respectively. For moderate and strong inter-core XT, it is obvious that the average BER of both unipolar OOK with a CI-based network and bipolar 2-PPM with a CI-based network is degraded compared to the single-core case in Fig. 5. However, unipolar OOK with a CI-based network exhibits the worst behavior. Indeed, by using bipolar 2-PPM together with the CI technique, the performance improves notably when it is compared to that of unipolar

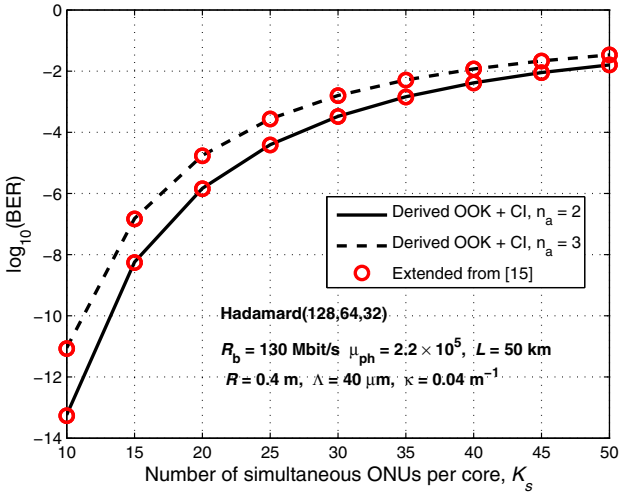

Fig. 4. Average BER of core-multiplexed SAC OCDMA PON adopting unipolar OOK for Hadamard (128,64,32) codes.

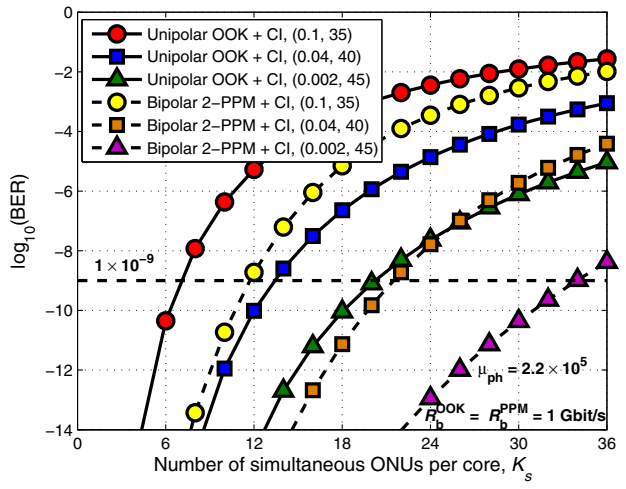

Fig. 6. Average BER performance of core-multiplexed OCDMA PON for different numbers of active ONUs per core.

OOK with a CI-based network. At $\kappa = 0.04$ m^{-1} (moderate inter-core XT), for example, unipolar OOK with a CI-based network supports 12 ONUs, while, by employing bipolar 2-PPM and CI, the number of supportable ONUs increased to 22 ONUs. These results prove the effectiveness of employing bipolar 2-PPM with CI compared to OOK to mitigate the inter-core XT impact. For weak inter-core XT, for which κ is set to 0.002 m^{-1}, the inter-core XT has negligible impact on the system performance for both unipolar OOK and bipolar 2-PPM.

Figure 7 shows the average BER performance of core-multiplexed SAC OCDMA PON versus the mean XT, μ_{XT} [dB/km], for both unipolar OOK with CI and bipolar 2-PPM with CI. The results are shown for $n_a = 3$, $\mu_{\text{ph}} = 2.2 \times 10^5$, and $L = 50$ km. At low mean XT values, the inter-core XT has a negligible impact on the performance of both networks, while keeping in mind the superiority of the bipolar 2-PPM scheme. Nevertheless, as μ_{XT} increases further, the inter-core XT diminishes the BER performance for both systems. It is clear from the figure that core-multiplexed SAC OCDMA PON employing bipolar 2-PPM with CI is more tolerant to inter-core XT than a unipolar OOK-based network. For instance, to keep BER $\leq 10^{-9}$ for $K_s = 20$ active ONUs per core, the mean XT should be below −37 and −22 dB/km for unipolar OOK with a CI-based network and bipolar 2-PPM with a CI-based network, respectively. Even with 30 active ONUs per core, a mean XT of about −29 dB/km can be tolerated by bipolar 2-PPM with a CI-based network.

Figure 8 evaluates the XT-limited attainable distance of core-multiplexed SAC OCDMA PON for both unipolar OOK with CI and bipolar 2-PPM with CI for different values of bending radius R when $\mu_{\text{ph}} = 2.2 \times 10^5$, $\Lambda = 40$ μm, $R_b = 1$ Gbit/s, and $n_a = 3$. For both systems, when increasing the transmission distance or the bending radius, the associated average BER degrades. This is because μ_{XT} exhibits a linear dependence on the fiber length and the bending radius [12]. It is clear from the figure that unipolar

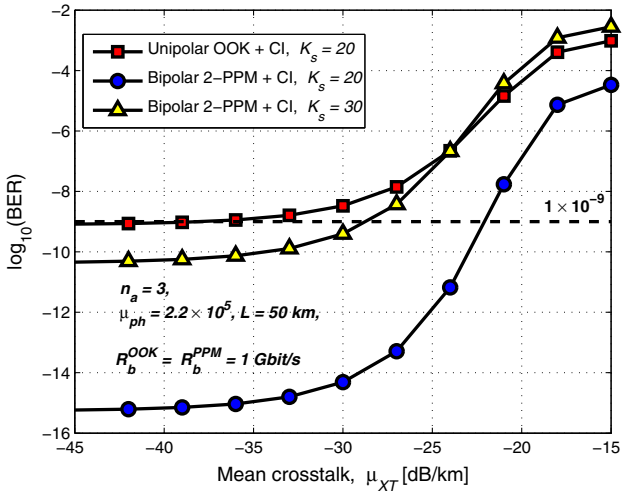

Fig. 7. Impact of mean crosstalk on the BER performance of core-multiplexed SAC OCDMA PON for the cases of unipolar OOK with CI and bipolar 2-PPM with CI when $n_a = 3$.

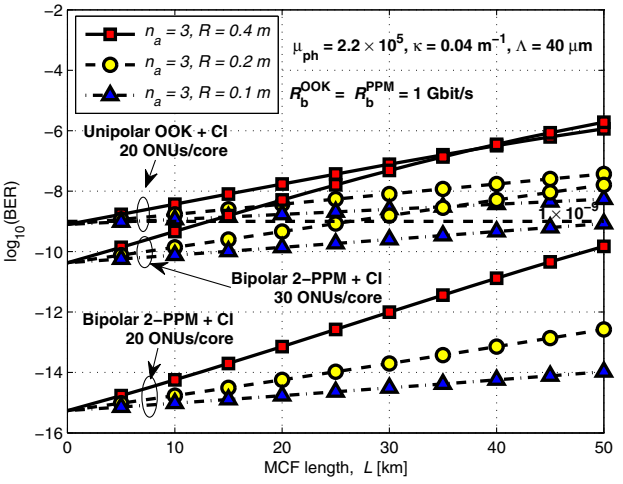

Fig. 8. Average BER of core-multiplexed SAC OCDMA PON versus fiber length for both unipolar OOK with CI and bipolar 2-PPM with CI when $R = 0.1, 0.2, 0.4$ m.

OOK with a CI-based network fails to reach a BER performance of 10^{-9} with 20 active ONUs per core, even with a short link length and a small bending radius. Meanwhile, for bipolar 2-PPM with a CI-based network with 20 active ONUs/core, a transmission reach exceeding 50 km is achievable, even with $R = 0.4$ m. For the case of bipolar 2-PPM with a CI-based network with 30 active ONUs per core and a bending radius of $R = 0.1$ m, the maximum transmission distance at BER $= 10^{-9}$ is limited to 50 km, whereas a transmission distance shortening of about 40% and 72% is found for the cases of $R = 0.2$ and 0.4 m, respectively.

Figure 9 shows the comparison between the core-multiplexed SAC OCDMA PON employing bipolar 2-PPM and CI and that employing conventional unipolar OOK with CI in terms of the maximum number of supportable ONUs per core for a BER $\leq 10^{-9}$ against the average photons per bit, μ_{ph}, and the mean XT, μ_{XT} [dB/km], where $R_b = 1$ Gbit/s, $L = 50$ km, and $n_a = 2, 3$. It can be seen that the maximum number of supportable ONUs decreases with increasing the mean XT and increases with the average photons per bit. We also notice that to achieve a particular average BER performance, bipolar 2-PPM signaling requires fewer photons as compared to unipolar OOK signaling, leading to an energy-efficient network. It is evident that the proposed schemes significantly improve both network capacity (in terms of the number of supportable users at a certain BER level) and the energy consumption compared to the OOK one. At $n_a = 2$, for example, Fig. 9(a) shows that unipolar OOK with a CI-based network could accommodate at most 20 ONUs per core for mean XT values as low as −37 dB/km and an average number of photons per bit of $\geq 2 \times 10^5$. Meanwhile, bipolar 2-PPM with a CI-based network can accommodate up to 33 ONUs per core for mean XT values lower than −35 dB/km and average number of photons per bit $\geq 1.3 \times 10^5$ [Fig. 9(c)]. Moreover, with mean XT as high as −28 dB/km and average photons as low as 0.8×10^5, 30 ONUs per core can be accommodated. Figures 9(b) and 9(d) also indicate that

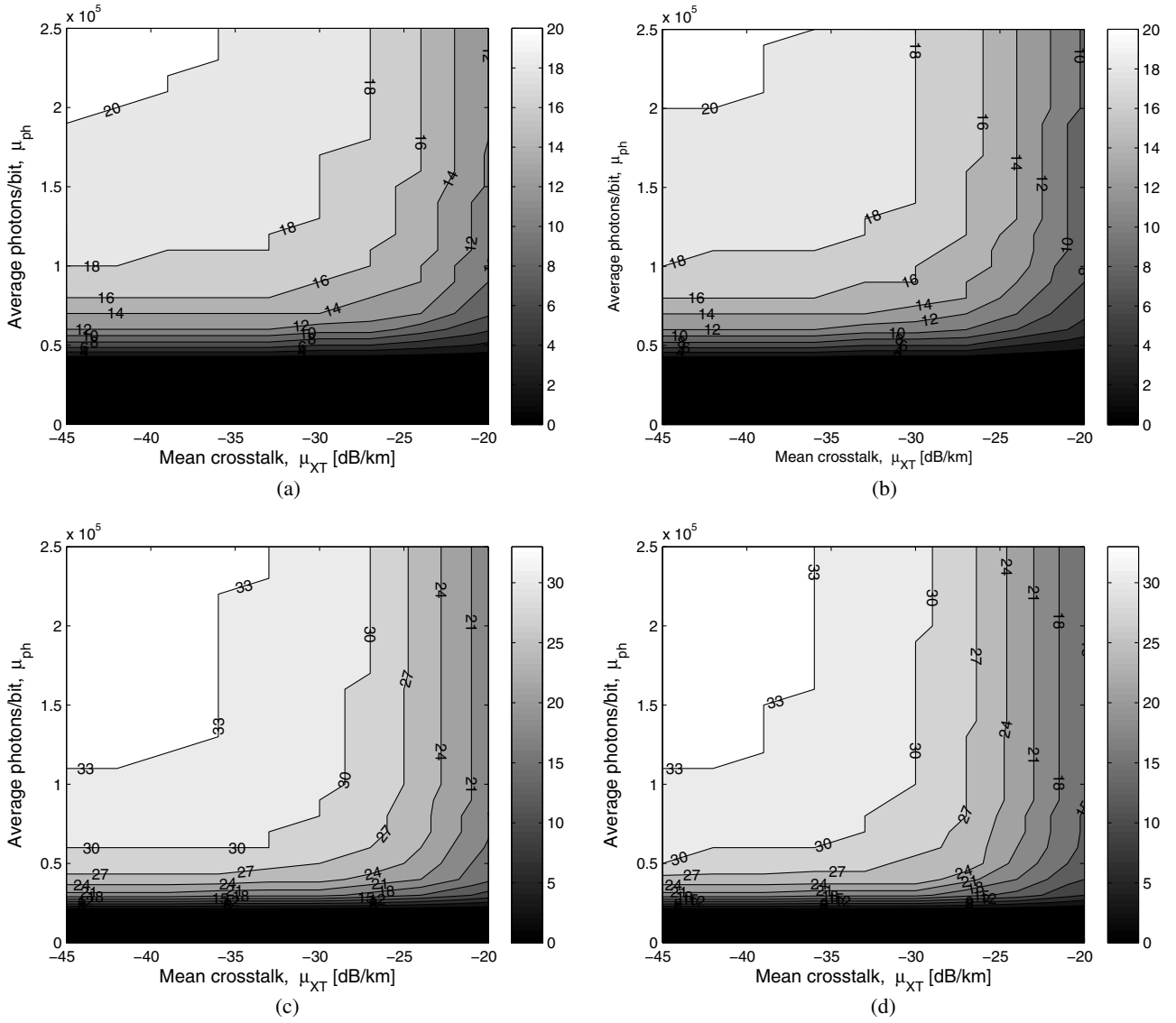

Fig. 9. Maximum number of supportable ONUs per core contours for a BER $\leq 10^{-9}$ against μ_{ph} and μ_{XT} [dB/km]. (a) Unipolar OOK + CI, $n_a = 2$; (b) unipolar OOK + CI, $n_a = 3$; (c) bipolar 2-PPM + CI, $n_a = 2$; and (d) bipolar 2-PPM + CI, $n_a = 3$.

about a 2 dB/km tolerable mean XT penalty is incurred at a BER of 10^{-9} with increasing the number of adjacent cores from 2 to 3.

V. Conclusion

In this paper, we have proposed a novel OLT architecture for core-multiplexed SAC OCDMA PONs based on the CI technique. The performance of the proposed technique was analyzed through deriving a closed-form BER expression in the presence of inter-core XT, beat noise, and receiver noise. A performance comparison with conventional core-multiplexed OCDMA PON that adopts unipolar OOK without CI reveals that CI not only simplifies the OLT implementation but also reduces the impact of inter-core XT, especially when the number of adjacent cores is large. In addition, we have proposed using bipolar 2-PPM signaling, which reduces the interaction time between co-propagating signals in adjacent cores for further performance improvement. The obtained results clearly show that bipolar 2-PPM with CI provides a superior performance over unipolar OOK with and without CI in terms of the number of accommodated ONUs and energy efficiency. The only price to be paid is additional 2×2 optical switches and delay elements at the OLT to perform 2-PPM modulation. Finally, the obtained results confirm that OCDMA PONs based on MCF emerge as promising candidates for future broadband access networks.

References

[1] Z. Feng, B. Li, M. Tang, L. Gan, R. Wang, R. Lin, Z. Xu, S. Fu, L. Deng, W. Tong, S. Long, L. Zhang, H. Zhou, R. Zhang, S. Liu, and P. Shum, "Multicore-fiber-enabled WSDM optical access network with centralized carrier delivery and RSOA-based

adaptive modulation," *IEEE Photon. J.*, vol. 7, no. 4, 1–9, Aug. 2015.

[2] C. Xiong, M. Tang, C. Ke, Z. Feng, and Q. Wu, "Experimental demonstration of ultra-dense WDM-PON with 7-core MCF enabled self-homodyne coherent detection," *IEEE Photon. J.*, vol. 9, no. 2, 1–7, Apr. 2017.

[3] C. Xia, N. Chand, A. Velázquez-Benítez, Z. Yang, X. Liu, J. Antonio-Lopez, H. Wen, B. Zhu, N. Zhao, F. Effenberger, R. Amezcua-Correa, and G. Li, "Time-division-multiplexed few-mode passive optical network," *Opt. Express*, vol. 23, no. 2, pp. 1151–1158, Jan. 2015.

[4] F. Ren, J. Li, T. Hu, R. Tang, J. Yu, Q. Mo, Y. He, Z. Chen, and Z. Li, "Cascaded mode-division-multiplexing and time-division-multiplexing passive optical network based on low modal-crosstalk FMF and mode MUX/DEMUX," *IEEE Photon. J.*, vol. 7, no. 5, 7903509, Oct. 2015.

[5] Y. Chen, J. Li, P. Zhu, Z. Wu, P. Zhou, Y. Tian, F. Ren, J. Yu, D. Ge, J. Chen, Y. He, and Z. Chen, "Novel MDM-PON scheme utilizing self-homodyne detection for high-speed/capacity access networks," *Opt. Express*, vol. 23, no. 25, pp. 32054–32062, Dec. 2015.

[6] T. Kodama, T. Isoda, K. Morita, A. Maruta, R. Maruyama, N. Kuwaki, S. Matsuo, N. Wada, G. Cincotti, and K. I. Kitayama, "First demonstration of a scalable MDM/CDM optical access system," *Opt. Express*, vol. 22, no. 10, pp. 12060–12069, May 2014.

[7] R. Matsumoto, T. Kodama, S. Shimizu, R. Nomura, K. Omichi, N. Wada, and K. I. Kitayama, "40G-OCDMA-PON system with an asymmetric structure using a single multi-port and sampled SSFBG encoder/decoders," *J. Lightwave Technol.*, vol. 32, no. 6, pp. 1132–1143, Mar. 2014.

[8] K. I. Kitayama, X. Wang, and N. Wada, "OCDMA over WDM PON-solution path to gigabit-symmetric FTTH," *J. Lightwave Technol.*, vol. 24, no. 4, pp. 1654–1662, Apr. 2006.

[9] A. E. Farghal, H. M. H. Shalaby, K. Kato, and R. K. Pokharel, "Performance analysis of multicode OCDM networks supporting elastic transmission with QoS differentiation," *IEEE Trans. Commun.*, vol. 64, no. 2, pp. 741–752, Feb. 2016.

[10] M. Kavehrad and D. Zaccarin, "Optical code-division-multiplexed systems based on spectral encoding of noncoherent sources," *J. Lightwave Technol.*, vol. 13, no. 3, pp. 534–545, Sept. 1995.

[11] A. E. Farghal, "Performance analysis of core-multiplexed spectral amplitude coded-OCDMA PON," *J. Opt. Commun. Netw.*, vol. 8, no. 9, pp. 666–675, Sept. 2016.

[12] T. Hayashi, T. Taru, O. Shimakawa, T. Sasaki, and E. Sasaoka, "Design and fabrication of ultra-low crosstalk and low-loss multi-core fiber," *Opt. Express*, vol. 19, no. 17, pp. 16576–16592, 2011.

[13] A. E. Farghal, H. M. H. Shalaby, K. Kato, and R. K. Pokharel, "Optical code-division multiplexing (OCDM) networks adopting code-shift keying/overlapping PPM signaling: Proposal and performance analysis," *IEEE Trans. Commun.*, vol. 63, no. 10, pp. 3779–3788, Oct. 2015.

[14] H. M. H. Shalaby, "Efficient use of PPM in spectral-amplitude-coding optical CDMA systems," *J. Lightwave Technol.*, vol. 30, no. 22, pp. 3512–3519, Nov. 2012.

[15] M. Noshad and K. Jamshidi, "Bounds for the BER of codes with fixed cross correlation in SAC-OCDMA systems," *J. Lightwave Technol.*, vol. 29, no. 13, pp. 1944–1950, July 2011.

[16] W. C. Kwong, P. A. Perrier, and P. R. Prucnal, "Performance comparison of asynchronous and synchronous code-division multiple-access," *IEEE Trans. Commun.*, vol. 39, no. 11, pp. 1625–1634, Nov. 1991.

[17] C.-C. Yang, "Optical CDMA passive optical network using prime code with interference elimination," *IEEE Photon. Technol. Lett.*, vol. 19, no. 7, pp. 516–518, Apr. 2007.

[18] T. Hayashi, T. Sasaki, and E. Sasaoka, "Behavior of inter-core crosstalk as a noise and its effect on Q-factor in multi-core fiber," *IEICE Trans. Commun.*, vol. E97.B, no. 5, pp. 936–944, May 2014.

[19] K. Takenaga, Y. Arakawa, S. Tanigawa, N. Guan, S. Matsuo, K. Saitoh, and M. Koshiba, "An investigation on crosstalk in multi-core fibers by introducing random fluctuation along longitudinal direction," *IEICE Trans. Commun.*, vol. E94-B, no. 2, pp. 409–416, Feb. 2011.

[20] B. J. Puttnam, R. S. Luis, T. A. Eriksson, W. Klaus, J.-M. Delgado Mendinueta, Y. Awaji, and N. Wada, "Impact of intercore crosstalk on the transmission distance of QAM formats in multicore fibers," *IEEE Photon. J.*, vol. 8, no. 2, 0601109, Apr. 2016.

[21] M. Rad and J. Salehi, "Phase-induced intensity noise in digital incoherent all-optical tapped-delay line systems," *J. Lightwave Technol.*, vol. 24, no. 8, pp. 3059–3072, Aug. 2006.

[22] R.-J. Essiambre, G. Kramer, P. J. Winzer, G. J. Foschini, and B. Goebel, "Capacity limits of optical fiber networks," *J. Lightwave Technol.*, vol. 28, no. 4, pp. 662–701, Feb. 2010.

[23] S. Matsuo, Y. Sasaki, T. Akamatsu, I. Ishida, K. Takenaga, K. Okuyama, K. Saitoh, and M. Kosihba, "12-core fiber with one ring structure for extremely large capacity transmission," *Opt. Express*, vol. 20, no. 27, pp. 28398–28408, Dec. 2012.

[24] B. Zhu, T. Taunay, M. Fishteyn, X. Liu, S. Chandrasekhar, M. Yan, J. Fini, E. Monberg, and F. Dimarcello, "112-Tb/s space-division multiplexed DWDM transmission with 14-b/s/Hz aggregate spectral efficiency over a 76.8-km seven-core fiber," *Opt. Express*, vol. 19, no. 17, pp. 16665–16671, 2011.